

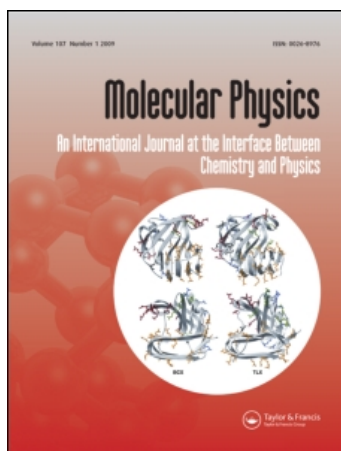
This article was downloaded by: [Meng, Sheng]

On: 21 July 2010

Access details: Access Details: [subscription number 924640209]

Publisher Taylor & Francis

Informa Ltd Registered in England and Wales Registered Number: 1072954 Registered office: Mortimer House, 37-41 Mortimer Street, London W1T 3JH, UK



## Molecular Physics

Publication details, including instructions for authors and subscription information:

<http://www.informaworld.com/smpp/title~content=t713395160>

### Optical properties of clusters and molecules from real-time time-dependent density functional theory using a self-consistent field

Jun Ren<sup>a</sup>; Efthimios Kaxiras<sup>a</sup>; Sheng Meng<sup>ab</sup>

<sup>a</sup> Institut des Matériaux, École Polytechnique Fédérale de Lausanne, CH-1015 Lausanne, Switzerland <sup>b</sup>

Beijing National Laboratory for Condensed Matter Physics, and Institute of Physics, Chinese Academy of Sciences, 100190 Beijing, China

Online publication date: 21 July 2010

**To cite this Article** Ren, Jun , Kaxiras, Efthimios and Meng, Sheng(2010) 'Optical properties of clusters and molecules from real-time time-dependent density functional theory using a self-consistent field', Molecular Physics, 108: 14, 1829 – 1844

**To link to this Article:** DOI: 10.1080/00268976.2010.491489

**URL:** <http://dx.doi.org/10.1080/00268976.2010.491489>

PLEASE SCROLL DOWN FOR ARTICLE

Full terms and conditions of use: <http://www.informaworld.com/terms-and-conditions-of-access.pdf>

This article may be used for research, teaching and private study purposes. Any substantial or systematic reproduction, re-distribution, re-selling, loan or sub-licensing, systematic supply or distribution in any form to anyone is expressly forbidden.

The publisher does not give any warranty express or implied or make any representation that the contents will be complete or accurate or up to date. The accuracy of any instructions, formulae and drug doses should be independently verified with primary sources. The publisher shall not be liable for any loss, actions, claims, proceedings, demand or costs or damages whatsoever or howsoever caused arising directly or indirectly in connection with or arising out of the use of this material.

## RESEARCH ARTICLE

# Optical properties of clusters and molecules from real-time time-dependent density functional theory using a self-consistent field

Jun Ren<sup>a</sup>, Efthimios Kaxiras<sup>a\*</sup> and Sheng Meng<sup>ab\*</sup>

<sup>a</sup>*Institut des Matériaux, École Polytechnique Fédérale de Lausanne, CH-1015 Lausanne, Switzerland;*

<sup>b</sup>*Beijing National Laboratory for Condensed Matter Physics, and Institute of Physics, Chinese Academy of Sciences, 100190 Beijing, China*

(Received 4 December 2009; final version received 30 April 2010)

We present a detailed study of optical absorption spectra of finite-size structures, using a method based on time-dependent density-functional theory (TDDFT), which involves a self-consistent field for the propagation of the Kohn–Sham wavefunctions in real-time. Although our approach does not provide a straightforward assignment of absorption features to corresponding transitions between Kohn–Sham orbitals, as is the case in frequency-domain TDDFT methods, it allows the use of larger timesteps while conserving total energy and maintaining stable dipole moment oscillations. These features enable us to study larger systems more efficiently. We demonstrate the efficiency of our method by applying it to a hydrogen-terminated silicon cluster consisting of 364 atoms, with and without P impurities. For cases where direct comparison to experiment can be made, we reproduce the absorption features of fifteen small molecules [N<sub>2</sub>, O<sub>2</sub>, O<sub>3</sub>, NO<sub>2</sub>, N<sub>2</sub>O, NH<sub>3</sub>, H<sub>2</sub>O, H<sub>2</sub>CO, H<sub>2</sub>CO<sub>3</sub>, CO<sub>2</sub>, CH<sub>4</sub>, C<sub>2</sub>H<sub>2</sub>, C<sub>2</sub>H<sub>4</sub>, C<sub>2</sub>H<sub>6</sub>, C<sub>6</sub>H<sub>6</sub>] and find generally good agreement with experimental measurements. Our results are useful for the detection and the determination of orientation of these molecules.

**Keywords:** optical absorption; TDDFT; nanoclusters; molecules

### 1. Introduction

Optical excitation of finite-size structures like molecules and clusters is one of the most fundamental and versatile methods for investigating their structure and stability, since experimental measurements can be linked to the electronic structure by careful analysis of the excitation spectrum. An ideal approach would employ a consistent theoretical framework and computational parameters to obtain the optical properties of systems of any size and composition. Such a general method is not currently available. Methods that can obtain very accurately the optical properties of very small systems of limited compositional variability do exist, but these methods cannot be applied to large systems because of their very high computational cost, which often scales exponentially with (or as a very large power of) system size. Methods that can handle large systems usually have to rely on approximations that sacrifice accuracy for the sake of efficiency, and can access the general trends of optical excitations but often cannot reproduce the details which are crucial for small systems. In this work we present an alternative approach bridging these two extremes, which should be a useful tool for investigating the optical properties of a wide range of finite-size structures.

In order to validate our approach, we apply it to the study of the optical properties of a representative group of small molecules, for which accurate experimental measurements exist. Application to a large atomic cluster, consisting of 220 Si and 144 H atoms, is also reported to demonstrate its efficiency. The optical properties of the molecules we chose to study are actually intrinsically interesting for a variety of reasons. Small molecules encountered in either high concentration (N<sub>2</sub>, O<sub>2</sub>, H<sub>2</sub>O, CO<sub>2</sub>) or low concentration (O<sub>3</sub>, NO<sub>2</sub>, NO, formaldehyde) in the Earth's atmosphere, play an important role in shielding living organisms from harmful solar ultraviolet (UV) radiation reaching the Earth's surface [1–3]; these molecules also play a role in modifying the composition of the atmosphere [4–7]. Some small hydrocarbons, including methane, ethane, acetylene, ethylene, and benzene, are crucial in the photochemistry of the Earth's upper atmosphere [6,8] and in various industrial applications. The UV absorption of these molecules is of particular interest, since they are activated under UV light.

Theoretical studies, based on *ab initio* quantum chemistry approaches, can easily provide a complete description of the energies, geometries, and dynamics of excited states of these small molecules with sufficient

\*Corresponding authors. Emails: efthimios.kaxiras@epfl.ch; smeng@iphy.ac.cn

accuracy and at a reasonable computational cost, without invoking any important approximations. Examples of such methods are configuration interaction (CI) [9], coupled cluster (CC) [10], and complete active space perturbation theory (CASPT) [11]. While the majority of previous such theoretical studies of small molecules focus on their atomic structure and electronic properties, some calculations of their excited states and photoabsorption spectra have also been reported [12]. These studies typically compare the excitation energies with experimental values but do not provide a detailed analysis of the relationship between absorption peaks and the corresponding electronic structure. As mentioned, these methods cannot usually be applied to large systems containing more than  $\sim 100$  atoms.

An alternative approach employs density functional theory (DFT) and its time-dependent version (TDDFT). Although an exact formulation, DFT/TDDFT in practical usage has to invoke approximations of the exchange-correlation effects among electrons [14–16]. The adiabatic approximation is usually employed in TDDFT approaches, and this is also the case in the present work. Compared to the high-level, computationally demanding methods, TDDFT in its current form has spectral accuracy close to that of the quantum chemical approaches (for example, CASPT, with exceptions in cases of charge transfer and multiple excitations) [13,17], and computational cost scaling as  $O(N^3)$  with  $N$  being the size of system, which is better than time-dependent Hartree–Fock theory [18,19]. We note here that the current form of TDDFT with adiabatic local or semilocal approximations does not offer an improvement over DFT description of excited states involving charge transfer, which is long ranged in nature, and double excitations [19,20]. Traditionally, TDDFT calculations are performed in the frequency domain [20–23] within the linear response approximation to an external field of a given frequency. The absorption spectra and oscillator strength are obtained by calculating the poles of the density–density response function. This approach has proven very successful in reproducing the observed vertical excitation energies and oscillator strength of small molecules, and has been pursued extensively in the last decade with various approximations for the exchange-correlation energy functionals [24–27] and types of basis-sets [25,28–30]. It has also been compared to different types of quantum chemistry methods [20,30,31]. In these cases, excited states in a small energy range, typically up to  $\sim 10$  eV, are calculated, since at higher excitation energies the number of fictitious electron–hole pairs increases significantly and the

frequency-domain TDDFT calculations become very difficult. Some fundamentals and application examples, together with a perspective on future challenges in TDDFT are provided in [32].

In contrast to the frequency-domain formulation of TDDFT, real-time propagation of wavefunctions [33–36] can produce the full absorption spectrum by a single calculation, albeit at the cost of a large number of propagation timesteps [33–35]. This type of TDDFT implementation for full-spectrum calculations has already been introduced by Rocca *et al.* [37]. In addition, a real-time approach has the advantage of automatically including non-linear effects since it does not rely on perturbation theory. A practical problem in real-time TDDFT calculations for finite-size structures, especially for polar ones such as water and ammonia, is that the electron density is very sensitive to the external field so that a very small timestep is needed to ensure the conservation of the total energy. In our approach we solve this problem by imposing a time-dependent self-consistent condition during the time evolution of Kohn–Sham (KS) wavefunctions. TDDFT simulations with a self-consistent field (SCF) are not new, and have been applied to electron dynamics [34] and implied in general procedures [35]. However, they have seldom been used for optical calculations [38] and their applicability in this domain has not been carefully examined. Here we apply this approach to the calculation of photoabsorption spectra of small molecules and demonstrate that it improves the efficiency of TDDFT without affecting its accuracy, thus making it feasible to explore efficiently a wide range of systems.

All of the optical absorption peaks for the molecules we studied are located in the region from 80 to 250 nm (15.5 to 4.96 eV), except for  $\text{NO}_2$  whose spectrum has a small peak around 367 nm (3.38 eV). We emphasise that our work does not focus on improving the accuracy of calculated excited energies for the selected molecules, which have already been the subject of extensive, higher level quantum chemistry calculations [24,26,30,31]. Therefore, an exhaustive comparison of the present results to previous calculations is not of interest here. Instead, we compare the overall features of our spectra with experimentally measured ones in a wide energy range (3–15 eV) and concentrate on the prominent absorption peaks (bright) rather than less important features (dark). Through these results, we elucidate the relationship between the optical absorption bands and the corresponding state transitions, based on calculated wavefunctions and transition dipole moments (TDM). The calculated TDM can be used to identify the molecules and their orientation based on electronic or optical information from each transition channel. Our results

provide a consistent reference point for comparison with optical absorption spectra measured in experiments, with which they are in generally good agreement. When possible, the calculated spectrum is also compared with previous TDDFT-based theoretical studies, which confirms that the accuracy of our approach is comparable to that of similar methods.

## 2. Computational methods

The first-principles calculations were carried out with the SIESTA code [40]. We use pseudopotentials of the Troullier–Martins type [41] to model the atomic cores, and the Ceperley–Alder form [42] of the local density approximation for the exchange–correlation functional, as parameterised by Perdew and Zunger [43]. Periodic boundary conditions with box sizes of 7–13 Å to minimise interactions with periodic images are employed to calculate Hartree energies. Larger unit cells do not alter our results due to the localised nature of atomic basis. An auxiliary real space grid equivalent to a plane-wave cutoff of 100 Ry is used. For geometry optimisation, a structure is considered fully relaxed when the magnitude of forces on the atoms is smaller than  $0.01 \text{ eV \AA}^{-1}$ . We use a basis of double-zeta polarised orbitals. For C, the basis set includes two radial functions to represent the  $2s$  states with confinement radii  $r_s = 5.12 \text{ au}$  and two additional  $2p$  shells plus a  $d$ -type polarisation shell for  $p$  electrons [44] with confinement radii  $r_p = r_p^{\text{Pol.}} = 6.25 \text{ au}$ , so that the total number of basis functions for a C atom is  $2 \times 1 + 2 \times 3 + 1 \times 5 = 13$ . The use of additional polarisation orbitals is necessary, since  $d$  polarisation functions are essential for TDDFT excitation energy calculations [30]. For N atoms we use a similar basis of 13 orbitals, including two  $2s$  shells, two  $2p$  shells, and a  $d$  orbital for  $p$ -electron polarisation with radii  $r_s = 4.50 \text{ au}$ , and  $r_p = r_p^{\text{Pol.}} = 5.50 \text{ au}$ , respectively. The number of orbitals for O is also 13, with two  $2s$  shells, two  $2p$  shells, and a  $d$  polarisation shell with confinement radii  $r_s = 3.93 \text{ au}$  and  $r_p = r_p^{\text{Pol.}} = 4.93 \text{ au}$ , respectively. For Si and P, thirteen numerical atomic basis: two  $3s$  shells with  $r_s = 5.01$  and  $4.56 \text{ au}$ , two  $3p$  shells and a  $4d$  polarisation shell with confinement radii  $r_p = r_p^{\text{Pol.}} = 6.27$  and  $5.57 \text{ au}$ , respectively, are considered. Finally, two radial shapes for the  $1s$  orbital and a  $p$ -type polarised orbital with confinement radii  $r_s = r_s^{\text{Pol.}} = 6.05 \text{ au}$  are employed for H. For the systems under study it was found that inclusion of additional shells (such as C  $3s$  orbitals) does not alter noticeably the results, nor does the partial core correction in pseudopotentials. The completeness of the basis is evident from the fact that the  $f$ -sum rule for all small molecules is in the 96–98% range.

We have modified the TDDFT scheme, used in earlier work to calculate optical absorption of small biological molecules like DNA bases [45,46] based on linear response, to include a self-consistent time propagation of the electron density. A self-consistent field has been used in TDDFT simulations of electron dynamics in small metal clusters [34] and has been proposed in general procedures of TDDFT propagation [35], but it has not been applied to the calculations of optical properties [38] and its validity and effectiveness remain unexamined. This approach, when applied to a photoabsorption calculation which is essentially within the linear response regime, proceeds as follows: at time  $t=0$ , an initial diagonalisation step is performed to obtain the Kohn–Sham wavefunctions for each orbital under a perturbative external electric field. The resulting KS eigenstates are denoted as  $\{\phi_j(0)\}$ , where  $j$  is the index of the occupied states. At  $t>0$ , the external field is switched off and the KS orbitals are allowed to evolve. The time propagation of  $\{\phi_j(t)\}$  is realised by multiplying it by the propagator  $\exp(-i\mathcal{H}[\rho, t_n] \Delta t)$ , at the  $n$ th step  $t_n = n\Delta t$ :

$$\phi_j(t_n + \Delta t) = \exp(-i\mathcal{H}[\rho, t_n] \Delta t) \phi_j(t_n). \quad (1)$$

Here  $\mathcal{H}$  is the DFT single-particle hamiltonian, including the kinetic energy operator,  $-(\hbar^2/2m)\nabla^2$ , and the electron–electron, electron–ion, and ion–ion interactions;  $\rho$  is the time-dependent density of electrons,  $\rho(t) = \sum_j |\phi_j(t)|^2$ , which enters the Hartree term (electron–electron repulsion) and the exchange–correlation term of the hamiltonian. The propagation of KS orbitals is based on the variation of TDDFT action functions in the adiabatic approximation. The detailed description of the self-consistency loop was presented in [47].

The TDDFT density evolution with the self-consistency loop increases significantly the stability of the simulation, therefore a longer timestep can be used. To illustrate these features, we report the results for the optical absorption spectrum of quinone-imine, an interesting biomolecule which is a key component of melanin [48]. This molecule has a small optical gap. In Figure 1(a) we compare the total energy of this molecule as a function of time during time evolution *with* and *without* the self-consistency loop, using a relatively large timestep,  $\Delta t = 0.0102 \text{ fs}$ . At time  $t < 0$  there is an electric field of  $0.1 \text{ V \AA}^{-1}$  applied along the short axis of the molecule, which is abruptly switched off at  $t = 0$ . In the regular time-propagation scheme without the self-consistency loop, the larger the timestep we use, the sooner the total energy of the system diverges; for  $\Delta t = 0.0102 \text{ fs}$ , this occurs around  $t = 12 \text{ fs}$ . When self-consistency is imposed by the scheme described above,

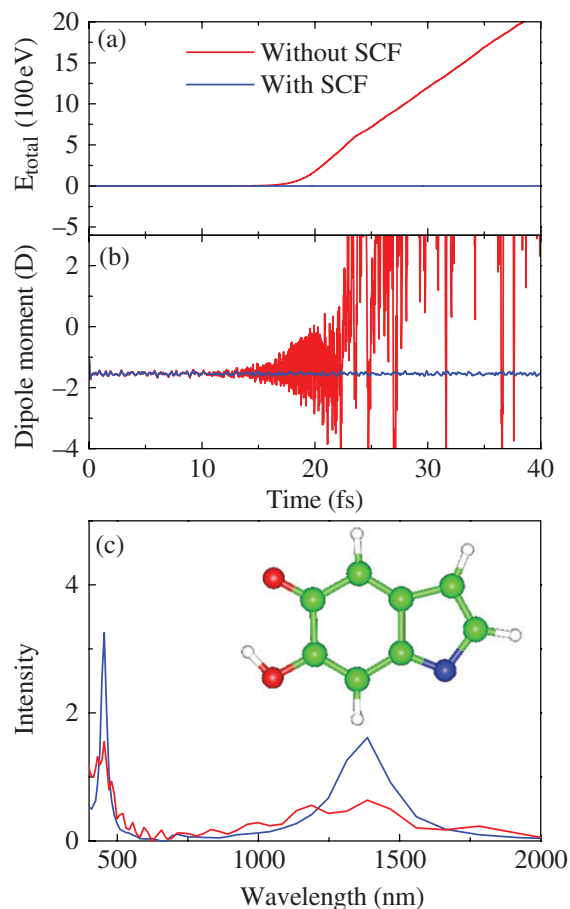


Figure 1. (a) Total energy; (b) dipole moment; and (c) optical spectrum of the quinone-imine molecule (structure shown in (c) inset), *without* (red lines) and *with* (blue lines) the self-consistency field (SCF) in TDDFT (for computational details see text).

we find that it leads to excellent total-energy conservation, with variations smaller than 1.5 meV (or 0.06% of the total energy) after 40 fs. This energy stability comes from the fact that the hamiltonian obtained with SCF,  $\mathcal{H}(\tau)$  ( $t_n < \tau \leq t_{n+1}$ ), approximates the exact one better than the hamiltonian without SCF,  $\mathcal{H}(t_n)$ , for the time span  $(t_n, t_n + \Delta t)$ .

The TDDFT propagation with a self-consistent field also results in long-time stability of the dipole moment oscillations of the system, which is particularly important for the low energy excitations. Stable dipole moment oscillation is maintained for a time interval exceeding 40 fs with SCF, while it starts to diverge at  $t = 12$  fs without SCF (see Figure 1(b)). As a result, the optical spectrum obtained from the Fourier transform of the dipole moment evolution is well converged with SCF, while the spectrum without SCF shows broader distribution and much more noise (Figure 1(c)). Although the optical absorption of this molecule has

not been directly measured, its very small optical gap of 0.9 eV (1378 nm) is consistent with the energy gap measured at  $1.2 \pm 0.2$  eV in melanin samples [49]. The second peak at 2.73 eV (454 nm) also agrees with the measured peak at 2.88 eV in melanin intermediates [48]. The computational cost for TDDFT with SCF is only  $\sim 2$  times that without SCF on average. As a result, the efficiency of the optical spectrum calculation is greatly enhanced, since the self-consistency loop allows a much larger timestep (by an order of magnitude or more). Typically, self-consistency is achieved at the cost of 1–3 iterations at each timestep. In addition, the longer total time span  $T$  of the simulation without energy divergence leads to enhanced resolution  $\Delta E$  in the optical spectrum, since  $\Delta E \sim h/T$  with  $h$  being Planck's constant. On the other hand, the timestep cannot be arbitrarily large because it then washes out the fast oscillations of the dipole moment, thus removing high-energy features of the absorption spectrum.

For the optical absorbance calculation within our modified TDDFT scheme, we use the Crank–Nicholson operator [47], a timestep of  $3.4 \times 10^{-3}$  fs and 6107 steps to propagate the wavefunctions for all molecules, which gives an energy resolution of 0.1 eV. This would not be possible with the regular time evolution method without the self-consistency loop, since the energy diverges early and the simulation fails at different timescales for different molecules. The perturbing external electric field we add on all the molecules is  $0.1 \text{ V \AA}^{-1}$ , for  $t < 0$ . For the  $\text{O}_2$  and  $\text{NO}_2$  molecules, spin polarisation is used to calculate the optical absorbance spectra. All calculations are performed in vacuum.

Frequency-domain TDDFT is often used to assign straightforwardly absorption peaks to transitions between occupied and virtual KS orbitals [21]. A proper assignment can also be obtained in real-time TDDFT by decomposing the dipole moment into contributions of each orbital [39]. Since our goal is to present a potentially useful self-consistent TDDFT approach for optical calculations of small and large finite systems, explicit assignments of absorption peaks for each molecule using the above approaches is not our focus here; instead, we use intuitive and simple ground-state transition dipole moment (TDM) calculations for such assignments to assist our understanding. We should note that this approach is based on fictitious single-particle KS orbitals to describe molecular states, therefore the reported molecular state wavefunctions, transition channels, and TDM are only valid in this context. In principle, high-level quantum chemistry methods can also be carried out for a more accurate, multi-configurational description of each molecular state.

In the present work, the assignment of absorption peaks obtained from TDDFT to specific excitation transitions in the molecular electronic structure was obtained by comparing to the peaks of the joint density of states weighted by the magnitude of the transition dipole moments calculated from DFT:

$$S_{\text{DFT}}(\omega) = \frac{2m\omega}{3e^2\hbar^2} \sum_{ij} n(\varepsilon_i)(1 - n(\varepsilon_j))\delta(\omega - \varepsilon_i - \varepsilon_j) |t_{i \rightarrow j}|^2, \quad (2)$$

where  $S_{\text{DFT}}(\omega)$  is the optical oscillator strength based on fictitious KS orbitals,  $e$  and  $m$  are the charge and mass of the electron,  $n(\varepsilon_{i,j})$  is the occupation of the KS eigenstate  $i$  ( $j$ ) with energy  $\varepsilon_{i,j}$ , with the indices  $i$  and  $j$  running over occupied and unoccupied states, respectively.  $t_{i \rightarrow j}$  is the transition dipole moment between the Kohn–Sham orbitals  $\phi_i(\mathbf{r})$  and  $\phi_j(\mathbf{r})$  in the ground-state configuration of the molecule, given by:

$$t_{i \rightarrow j} = \langle \phi_j(\mathbf{r}) | \mathbf{r} | \phi_i(\mathbf{r}) \rangle. \quad (3)$$

The DFT calculations give main peaks of the optical absorption spectrum which exhibit a pattern similar to that obtained from the real-time TDDFT simulation. In the DFT calculation, the peak position is the energy difference between a pair of KS orbitals and the intensity is proportional to the square of the TDM. The comparison of the two spectra is discussed in more detail for the cases of the ozone and water molecules, in the following section. Through this comparison, we can clearly identify the excitation transition to which a particular peak in the TDDFT optical absorption spectrum corresponds. When the spectrum includes many closely spaced peaks this procedure becomes problematic, and one can refer to more straightforward methods discussed above, but for all the cases studied here it is a simple procedure.

### 3. Results and discussion

We begin with an example which clearly demonstrates the computational efficiency of our self-consistency scheme through the calculation of the optical absorption spectrum of a rather large system by the present standards. We have considered a cluster that contains 220 Si atoms and 144 H atoms at the surface, which are used to saturate the Si dangling bonds, in an approximately spherical shape with a diameter of 2 nm. Si nanocrystals of this size range have become the subject of interest recently because of their potentially useful applications in nano-scale devices. Issues related to their electronic and optical excitations are of central importance in their potential usefulness (see, for

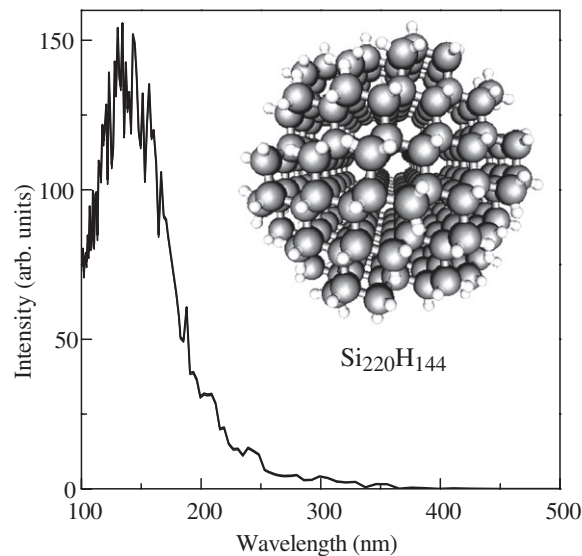


Figure 2. Optical spectrum of the  $\text{Si}_{220}\text{H}_{144}$  cluster obtained from TDDFT with the SCF. Atomic structure is shown in the inset, with grey spheres representing Si atoms and white spheres representing H atoms.

example, [50]). Therefore, being able to calculate the optical and electronic spectrum of such structures efficiently and accurately becomes of paramount importance in determining their properties. The optical spectrum of this model Si nanocrystal is shown in Figure 2. The calculation required 2100 steps (with a timestep  $\Delta t = 0.0102$  fs) and a total computational time 140 cpu hours on an Opteron single-node. The calculated overall shape and optical gap of  $\sim 3.0$  eV are consistent with previous calculations and experiments on clusters of similar size (2.6–3.2 eV) [51,52]. Without the SCF loop, the calculation of the optical spectrum with comparable resolution would require a computational time larger by approximately one order of magnitude.

To further demonstrate the efficiency and accuracy of our approach, we also considered the effects of doping of the model Si cluster, by replacing two Si atoms near the centre of the cluster by two P dopant atoms. The two P impurity atoms are placed at a distance of 4.56 Å, and the structure of the cluster was optimised by energy minimisation. Figure 3(a) shows the density of states of the P-doped Si cluster: two additional states separated by 0.1 eV, are introduced by the P dopants in the gap region close to the bottom of the unoccupied states. One of the two gap states is fully occupied while the other one is empty. These observations are consistent with the intuition that substitutional P dopants will donate one electron each forming electron trap states. Optical spectrum calculations were performed using our TDDFT scheme with the

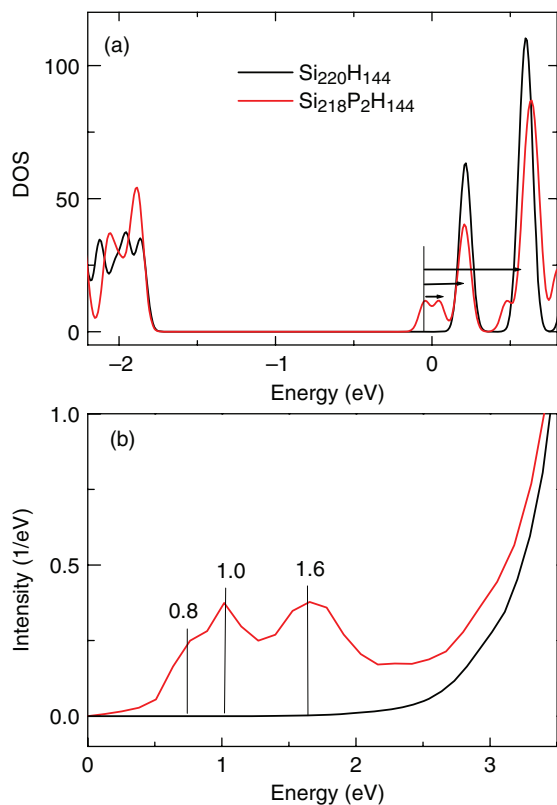


Figure 3. (a) Density of states (DOS) for the  $\text{Si}_{220}\text{H}_{144}$  cluster (black line) and the  $\text{Si}_{218}\text{P}_2\text{H}_{144}$  (red line) which contains two P dopants near its centre. The zero of the energy scale is set to the Fermi level. (b) Corresponding low-energy optical absorption spectra calculated from TDDFT. The absorption peaks at 0.8, 1.0, and 1.6 eV are assigned to the transitions between electronic states indicated by arrows in (a).

self-consistent field. The spectrum is essentially identical with that of the undoped cluster which was presented in Figure 2, except in the low energy region ( $<3$  eV). A comparison of the spectra for doped and undoped clusters in the low-frequency region where they differ significantly is shown in Figure 3(b). It is clear that three peaks show up in the low energy region (infrared to visible), at 0.8, 1.0, and 1.6 eV, respectively. They are assigned to the optical transitions starting from the occupied impurity state, to the unoccupied impurity state, and to low-energy unoccupied cluster states, as indicated by horizontal arrows in Figure 3(a). This example explicitly demonstrates that our method can be routinely applied to study optical properties of semiconductor clusters comprising several hundreds of atoms, providing accurate insight to the optical and electronic properties of such systems. For comparison, calculating absorption spectrum (which, in this model system, has an absorption maximum at  $\sim 8$  eV) for atomic clusters and impurity dopants of similar size would be a daunting task for frequency domain

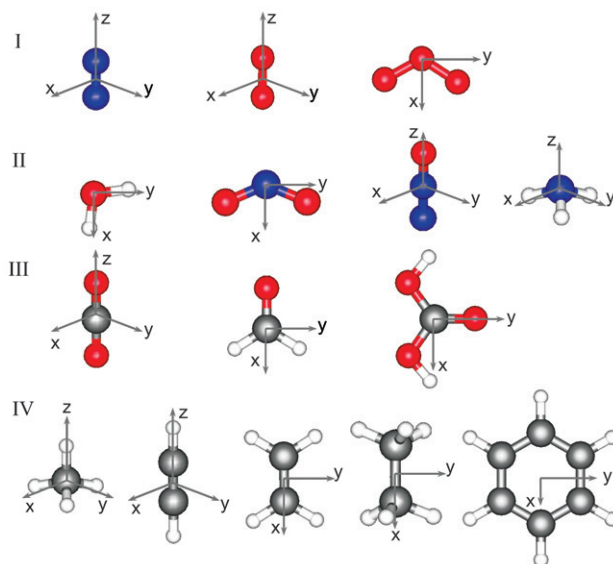


Figure 4. The geometry of the fifteen small molecules studied, in four groups (I–IV) as discussed in the text; Group I:  $\text{N}_2$ ,  $\text{O}_2$ ,  $\text{O}_3$ ; Group II:  $\text{H}_2\text{O}$ ,  $\text{NO}_2$ ,  $\text{N}_2\text{O}$ ,  $\text{NH}_3$ ; Group III:  $\text{CO}_2$ ,  $\text{H}_2\text{CO}$ ,  $\text{H}_2\text{CO}_3$ ; Group IV:  $\text{CH}_4$ ,  $\text{C}_2\text{H}_2$ ,  $\text{C}_2\text{H}_4$ ,  $\text{C}_2\text{H}_6$ ,  $\text{C}_6\text{H}_6$ . Red, white, grey, and blue spheres denote the oxygen, hydrogen, carbon, and nitrogen atoms, respectively.

TDDFT and wavefunction-based quantum chemistry methods.

We next consider the small molecules mentioned in the introduction, for which detailed experimental and theoretical results are readily available for comparison. Based on the different chemical composition and complexity of the molecules we studied, we divide them into four groups: Group I, consisting of  $\text{N}_2$ ,  $\text{O}_2$ , and  $\text{O}_3$ , are the simplest elemental molecules; Group II,  $\text{NO}_2$ ,  $\text{N}_2\text{O}$ ,  $\text{NH}_3$ , and  $\text{H}_2\text{O}$ , are the simple bi-elemental compounds composed of N, O, and H; Group III,  $\text{H}_2\text{CO}$ ,  $\text{H}_2\text{CO}_3$ , and  $\text{CO}_2$ , are the carbon oxides; and Group IV,  $\text{CH}_4$ ,  $\text{C}_2\text{H}_2$ ,  $\text{C}_2\text{H}_4$ ,  $\text{C}_2\text{H}_6$ , and  $\text{C}_6\text{H}_6$ , are the hydrocarbons. The ground state geometry for each of these molecules is shown in Figure 4. We will first discuss the general optical properties for these four groups of molecules, then we choose a few representative molecules in each group for a more detailed discussion. A compilation of optical absorption spectra for representative cases is shown in Figure 5.

**Group I:** the  $\text{O}_2$  and  $\text{N}_2$  molecules show two dominant absorbance bands in the UV region. The positions of the second peak for both molecules are very close, around 83 nm, although with very different intensity. The first peak for  $\text{O}_2$  is located at 139 nm, different from that for  $\text{N}_2$ , which is at 95 nm. The differences can be attributed to features of the electronic structure of the two molecules: the strong triple-bond between

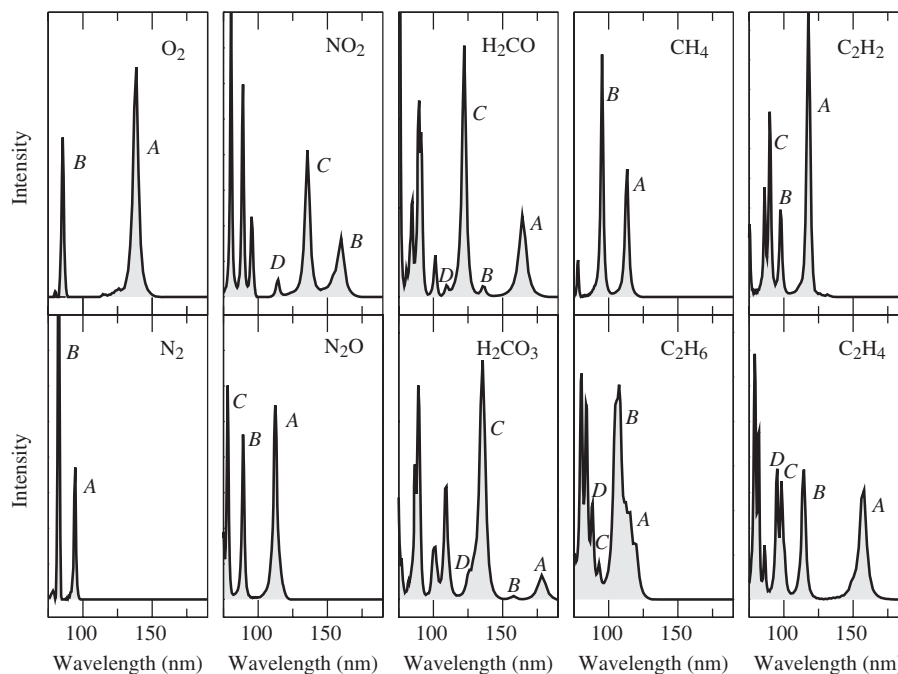


Figure 5. The calculated absorption spectra for several small molecules in the 80 to 200 nm range. For  $\text{NO}_2$ , the first absorption peak, *A*, lies outside the range shown.

the two N atoms in  $\text{N}_2$  is related to the stronger absorbance at the higher energy (83 nm), while the presence of the triplet electronic states in  $\text{O}_2$  results in a lower-energy transition at 139 nm.

**Group II:** the first peak of the  $\text{N}_2\text{O}$  molecule, compared to the first peak of  $\text{N}_2$ , is red-shifted to 112 nm, due to the presence of the O atom. The other two peaks are located at similar positions as those for  $\text{N}_2$ , suggesting a similar origin in electronic transitions. Overall, the oscillator strength (intensity) is enhanced relative to  $\text{N}_2$ , indicating a larger polarisability in this region. In the  $\text{NO}_2$  molecule, the first peak has a large shift to 367 nm with a small intensity, and the other three absorbance bands are evenly distributed in the region from 100 to 160 nm.

**Group III:** for the  $\text{H}_2\text{CO}$  and  $\text{H}_2\text{CO}_3$  molecules, the trends for the intensity of the first four bands are similar in both cases, that is, alternating large–small–large–small peaks with decreasing wavelength. With the presence of more O atoms, the peaks of  $\text{H}_2\text{CO}_3$  are red-shifted by  $\sim 14$  nm, accompanied by a sharp decrease in the intensity of the first peak.

**Group IV:** two peaks, at 95 nm (13.02 eV) and 113 nm (10.93 eV), are prominent in the UV spectrum of the simplest of the hydrocarbon molecules,  $\text{CH}_4$ . They are close to experimental values [53] of 13.6 and 10.4 eV. It seems that the first peak in experiment at 9.6 eV is missing or mixed with the peak at 10.93 eV in Figure 5.

The calculated oscillator strength for the first peak, integrated from 106 to 124 nm, is 0.401, in very good agreement with experimental value 0.4 [56]. In the literature, the low energy excitation in  $\text{CH}_4$  at 9–11 eV has been assigned to Rydberg transitions to states that involve C 3s orbitals [57]. The explicit inclusion of C 3s orbitals in basis-set, however, does not change the spectrum at low energy  $< 15$  eV in the present work. This question is open to further investigation.  $\text{C}_2\text{H}_6$  has similar peaks in its absorption spectrum to those of  $\text{CH}_4$ , except that each peak is split into two due to the presence of two  $\text{CH}_3$  groups connected by a C–C bond and smeared out. The optical spectra of molecules  $\text{C}_2\text{H}_4$  and  $\text{C}_2\text{H}_6$  exhibit similar overall trends. The C=C double bond in the  $\text{C}_2\text{H}_4$  molecule leads to a large red-shift in the position of the first band compared to the  $\text{C}_2\text{H}_6$  molecule, and the other three peaks are red-shifted by a smaller amount. Compared to the spectrum of  $\text{C}_2\text{H}_4$ , the C $\equiv$ C triple bond of  $\text{C}_2\text{H}_2$  results in a large increase in intensity for its first absorption peak without significant change in the peak position. However, a new peak with a significant red-shift is present at 158 nm for the case of  $\text{C}_2\text{H}_4$ , due to the transition from a triple bond to a double bond. At higher energy, absorption peaks show similar features for the two molecules  $\text{C}_2\text{H}_2$  and  $\text{C}_2\text{H}_4$ . The calculated excitation energy (158 nm) and oscillator strength (0.324) for the first peak of  $\text{C}_2\text{H}_2$  are very close to corresponding experimental values (161 nm and 0.30, respectively) [56].

Table 1. Absorption bands, corresponding transitions, and transition dipole moments for CH<sub>4</sub>, C<sub>2</sub>H<sub>2</sub>, C<sub>2</sub>H<sub>4</sub>, C<sub>2</sub>H<sub>6</sub>, and C<sub>6</sub>H<sub>6</sub>. (D<sub>x</sub>, D<sub>y</sub>, D<sub>z</sub>)<sup>§</sup> denotes two dipole moments (D<sub>x</sub>, D<sub>y</sub>, D<sub>z</sub>) and (-D<sub>z</sub>, D<sub>y</sub>, D<sub>x</sub>); (D<sub>x</sub>, D<sub>y</sub>, D<sub>z</sub>)<sup>-</sup> denotes two dipole moments (D<sub>x</sub>, D<sub>y</sub>, D<sub>z</sub>) and (-D<sub>x</sub>, -D<sub>y</sub>, D<sub>z</sub>); (D<sub>x</sub>, D<sub>y</sub>, D<sub>z</sub>)<sup>△</sup> denotes dipole moments (D<sub>x</sub>, D<sub>y</sub>, D<sub>z</sub>) and (-D<sub>y</sub>, -D<sub>x</sub>, D<sub>z</sub>); (D<sub>x</sub>, D<sub>y</sub>, D<sub>z</sub>)<sup>∅</sup> means (D<sub>x</sub>, D<sub>y</sub>, D<sub>z</sub>) and (-D<sub>x</sub>, D<sub>y</sub>, D<sub>z</sub>); (D<sub>x</sub>, D<sub>y</sub>, D<sub>z</sub>)<sup>⊕</sup> means (D<sub>x</sub>, D<sub>y</sub>, D<sub>z</sub>) and (D<sub>x</sub>, D<sub>z</sub>, D<sub>y</sub>); (D<sub>x</sub>, D<sub>y</sub>, D<sub>z</sub>)<sup>⊖</sup> means (D<sub>x</sub>, D<sub>y</sub>, D<sub>z</sub>) and (D<sub>x</sub>, -D<sub>z</sub>, D<sub>y</sub>); and (D<sub>x</sub>, D<sub>y</sub>, D<sub>z</sub>)<sup>⊙</sup> means the four channels obtained from combining (D<sub>x</sub>, D<sub>y</sub>, D<sub>z</sub>)<sup>⊕</sup> and (D<sub>x</sub>, D<sub>y</sub>, D<sub>z</sub>)<sup>⊖</sup>. Other definitions are the same as in Tables 2–4. Axial directions of these molecules are defined in Figure 4 (Group IV).

	Band	$E_{\text{abs}}(\text{eV})$		Assignment	Transition dipole moments			$N$	
		Exp.	The.		D <sub>x</sub>	D <sub>y</sub>	D <sub>z</sub>		
CH <sub>4</sub>	A	9.60; 10.40 [53]	10.93	H → L	-0.05	0	-0.64	§	2
					0	0.65	0		1
	B	13.60	13.02	H → L+1	-0.61	0	0.43		1
					0.26	0	0.70		1
					0.40	0	-0.49		1
					0	0.71	0		1
					0	-0.64	0		1
C <sub>2</sub> H <sub>2</sub>	A	9.50 [54]	10.54	H → L	-0.71	0	-0.38	*	1
					0	0	0.31		2
	B	13.50	12.72	H → L+3	0	0	-1.30	△	2
					0.55	-0.56	0		2
	C	15.50	13.82	H-1 → L+1	0	0	-1.10	*	1
					0.66	0.41	0		2
					0.66	0.41	0		2
C <sub>2</sub> H <sub>4</sub>	A	7.40 [55]	7.85	H → L	-1.41	0	0		1
					-0.96	0	0		1
	B	9.90	10.83	H-1 → L+2	0	-0.85	0		1
					0	-0.85	0		1
					0	-0.85	0		1
	C	12.40	12.62	H-2 → L+2	0	-0.79	0		1
					0	-0.79	0		1
-0.74					0	0	1		
0					0.97	0	1		
0					0	-0.79	1		
C <sub>2</sub> H <sub>6</sub>	A	9.40; 10.70 [53]	10.33	H → L+1	0	0	-0.58	⊙	4
					0.76	-0.48	0		2
	B	11.60	11.53	H-1 → L+1	-0.88	0	0	∅	1
					0	0	0.60		2
					0	0	-0.75		2
					0	0	0.60		2
					0	0	0.60		2
C	14.50	14.01	H-1 → L+4	-1.07	0	0	⊙	1	
				0	0	0.72		4	
				0	0	0.72		4	
				0	0	0.72		4	
C <sub>6</sub> H <sub>6</sub>	A	6.94 [8]	6.96	H → L	-0.10	1.46	0	-	2
					1.46	0.10	0		2
	B	8.39; 9.16	8.35	H-1 → L	0	0	0.10	*	2
					0	0	0.17		2
	C	10.50	10.24	H → L+2	0	0	0.17	*	2
					0	0	-0.04		2
					0	0	-0.04		2
D	11.10	11.13	H-1 → L+2	0.55	0.00	0	-	2	
				0.00	0.55	0		2	

In Tables 1–4, we compare our theoretical excitation energies obtained from TDDFT with available experimental values. Our results are generally in good agreement with the experimental data for these molecules. Our spectra cannot be directly compared with some earlier TDDFT calculations performed in the frequency domain [24,28] since many states reported in such calculations are ‘dark’ and no oscillator strength is presented. We do find some excitation energies which coincide, within a tolerance of 0.2–0.4 eV, between our results and earlier calculations, when referring to the same state. More importantly, our results represent a complete set of electron excitations

within a consistent theoretical treatment, which provides not only the unbiased excitation energies but also the corresponding transitions between electronic states, TDMs and number of excitation channels. This information can help interpret optical spectra measured in experiment and the electronic properties of these molecules.

We next choose a few representative molecules from each group and analyse in detail the spectral features, the wavefunctions, the electronic excitation channels, and the corresponding TDMs. The molecules we chose are: ozone, which is responsible for absorbing UV light in the stratosphere, and thus shielding biological

Table 2. Absorption bands, corresponding transitions between electronic states, and transition dipole moments for the molecules  $N_2$ ,  $O_2$  and  $O_3$ . The experimental and theoretical energies of maximum absorption ( $E_{\text{abs}}$ ) are listed. ‘H’ and ‘L’ stand for the highest occupied molecular orbitals (HOMO) and the lowest unoccupied molecular orbitals (LUMO), respectively, and corresponding states below ( $H-1, \dots$ ) and above ( $L+1, \dots$ ) these levels. For transition dipole moments,  $N$  denotes the number of channels during the transition.  $(D_x, D_y, D_z)^*$  denotes two dipole moments  $(D_x, D_y, \pm D_z)$ ;  $(D_x, D_y, D_z)^\dagger$  denotes two dipole moments  $(D_x, D_y, D_z)$  and  $(D_y, -D_x, D_z)$ ; and  $(D_x, D_y, D_z)^\ddagger$  means two dipole moments  $(D_x, D_y, D_z)$  and  $(D_y, D_x, D_z)$ . Degenerate channels not affiliated with any symbols denote two or more channels which have the same transition dipole moments. Axial directions of these molecules are defined in Figure 4 (Group I). Only the relative magnitude of the dipole components are meaningful, since DFT calculations overestimate the actual dipole moment.

Band	$E_{\text{abs}}(\text{eV})$		Assignment	Transition dipole moments			$N$	
	Exp.	The.		$D_x$	$D_y$	$D_z$		
$N_2$	<i>A</i>	12.93; 13.21 [4]	13.12	$H-1 \rightarrow L$	0	0	0.77	
					0	0	0.76	*
$O_2$	<i>B</i>	14.23	15.01	$H-2 \rightarrow L$	0.20	-0.72	0	†
					0	0	1.10	
$O_3$	<i>A</i>	8.72 [1]	8.95	$H \rightarrow L$	0	0	0.38	*
					0	0	0	‡
	<i>B</i>	14.51	14.51	$H-2 \rightarrow L$	0.34	0.56	0	
					0	1.69	0	
<i>C</i>	4.86 [1]	5.37	$H-2 \rightarrow L$	0	0.70	0		
				9.31	9.14	$H-1 \rightarrow L+1$	0	0.70
<i>D</i>	10.21; 10.59	10.93	$H-5 \rightarrow L$	0.60	0	0		
				11.10	11.63	$H \rightarrow L+2$	0	0.94

Table 3. Absorption bands, transitions, and dipole moments for  $NO_2$ ,  $N_2O$ , and  $H_2O$ . For transition dipole moments,  $(D_x, D_y, D_z)^*$  denotes two dipole moments  $(D_x, D_y, D_z)$  and  $(-D_y, D_x, D_z)$ . Other definitions are the same as in Table 2. Molecular axial directions are defined in Figure 4 (Group II).

Band	$E_{\text{abs}}(\text{eV})$		Assignment	Transition dipole moments			$N$	
	Exp.	The.		$D_x$	$D_y$	$D_z$		
$NO_2$	<i>A</i>	3.18 [58]	3.38	$H-1 \rightarrow L$	0	-1.24	0	
					0	-1.51	0	
	<i>B</i>	7.38 [59]	7.75	$H-4 \rightarrow L+1$	0	1.50	0	
					0	0.65	0	
<i>C</i>	8.67; 9.69 [59]	9.14	$H-5 \rightarrow L$	-0.59	0	0		
				0	0	0		
$N_2O$	<i>D</i>	10.92 [59]	10.83	$H-10 \rightarrow L+1$	0.48	0	0	
					0	0	1.63	
	<i>A</i>	9.65 [3]	11.03	$H \rightarrow L$	0	0	0	*
					-0.42	0.13	0	*
<i>B</i>	11.52	13.91	$H-1 \rightarrow L$	-0.46	0.15	0		
				0	0	-0.77		
$NH_3$	<i>C</i>	8.67; 9.69 [59]	9.14	$H-3 \rightarrow L$	0	0	0	
					0	0	0.47	
	<i>A</i>	6.46 [7]	6.96	$H \rightarrow L$	0	0	0	
					-0.32	0	0	†
<i>B</i>	9.18	9.24	$H \rightarrow L+1$	-0.68	0	0	‡	
				0.167	0	0	‡	
$H_2O$	<i>C</i>	11.37	12.13	$H-1 \rightarrow L$	0	0	0.32	
					0	0	0	
	<i>D</i>	14.31	14.31	$H \rightarrow L+2$	0.167	0	0	‡
					0	0	0	
<i>A</i>	7.45 [2]	7.55	$H \rightarrow L$	0	0	0.32		
				0.39	0.39	0		
<i>B</i>	9.67	9.74	$H-1 \rightarrow L$	-0.32	0.32	0		
				0.51	-0.51	0		
<i>C</i>	11.93	11.93	$H-1 \rightarrow L+1$	-0.32	0.32	0		
				0.51	-0.51	0		
<i>D</i>	13.72	13.72	$H-2 \rightarrow L$	0.51	-0.51	0		
				0.51	-0.51	0		

structures like DNA from radiation damage; water, which is ubiquitous on Earth and is one of the basic molecules involved in sustaining life and many other important processes; ammonia, which plays a significant role in industrial manufacturing, fertiliser synthesis, and has a major environmental impact, for example,

in crop growth; carbon dioxide, which is the product in every oxidation reaction of carbon-containing molecules and plays a major role in the Earth's balance of energy with direct consequences on the global climate; and benzene, an important hydrocarbon used in the production of many industrial chemicals, which has

Table 4. Absorption bands, transitions, and dipole moments for molecules  $\text{H}_2\text{CO}$ ,  $\text{H}_2\text{CO}_3$ , and  $\text{CO}_2$ . All definitions are the same as in Table 2. Axial directions of these molecules are defined in Figure 4 (Group III).

	Band	$E_{\text{abs}}(\text{eV})$		Assignment	Transition dipole moments			$N$	
		Exp.	The.		$D_x$	$D_y$	$D_z$		
$\text{H}_2\text{CO}$	$A$	7.20; 8.10 [5]	7.55	$\text{H} \rightarrow \text{L}+1$	0	-0.68	0	1	
				$\text{H}-1 \rightarrow \text{L}$	-1.13	0	0	1	
	$B$	9.05	9.14	$\text{H}-2 \rightarrow \text{L}$	0	0	0.09	1	
$\text{H}_2\text{CO}_3$	$C$	9.74	10.14	$\text{H} \rightarrow \text{L}+2$	0.82	0	0	1	
	$A$		6.96	$\text{H} \rightarrow \text{L}+1$	0.46	0	0	1	
				$\text{H}-1 \rightarrow \text{L}$	0	1.22	0	1	
	$B$		7.85	$\text{H} \rightarrow \text{L}+2$	0	-0.23	0	1	
	$C$		9.14	$\text{H}-2 \rightarrow \text{L}$	0.94	0	0	1	
$\text{CO}_2$	$A$	11.05; 11.40 [4]	12.42	$\text{H} \rightarrow \text{L}$	0	0	1.41	*	2
					0	0	-0.11	†	2
	$B$	13.78	14.71	$\text{H}-3 \rightarrow \text{L}$	-0.04	-0.58	0		2
	$C$	16.23	15.41	$\text{H}-1 \rightarrow \text{L}+1$	0	0	0.78		1

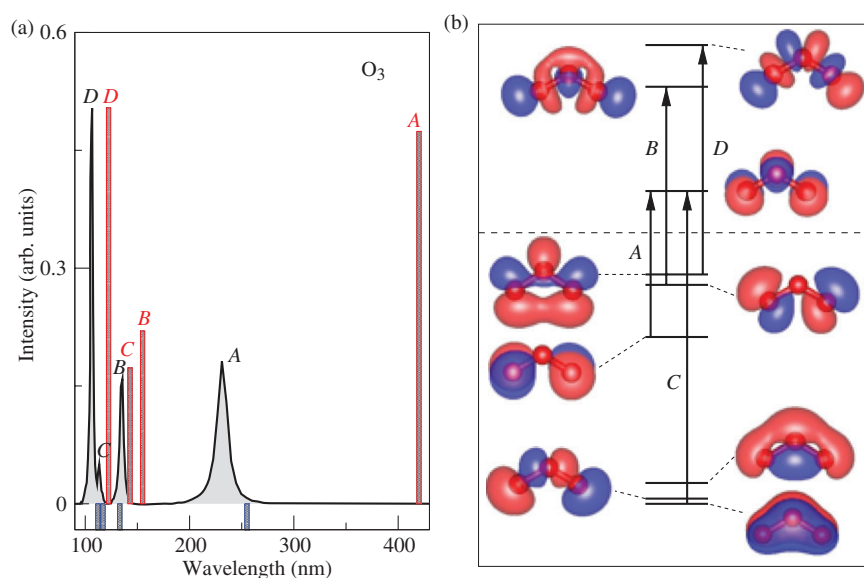


Figure 6. Ozone molecule. (a) Absorption spectrum; the red bars represent the peaks of  $S_{\text{DFT}}(\omega)$ , Equation (2), which help identify the nature of the TDDFT peaks, and are scaled so that the heights of the dominant peak ( $D$ ) from the two calculations match. (b) Energy level diagram and transitions corresponding to the absorption peaks; for each energy level, the corresponding wavefunction is shown as blue (positive) and red (negative) iso-electronic contours. The atomic positions are indicated by spheres with the same convention as in Figure 2. The letters in (b) identify the transitions that correspond to labelled peaks in (a). In this and the following figures, black vertical arrows represent single-channel electronic transitions between two states and thicker blue arrows represent multiple-channel transitions (for ozone all transitions are single-channel). The small blue bars below the zero intensity line indicate the position of experimental peaks.

very interesting electronic structure, exhibiting delocalised states and resonance. The optical transitions we considered in these molecules are from the highest occupied molecular orbital (HOMO or simply H in the tables) and states below it in energy, labelled H-1, H-2, etc. in order of decreasing energy, to the lowest unoccupied molecular orbital (LUMO or simply L in the tables) and states above it in energy, labelled L+1,

L+2, etc. in order of increasing energy. When there is a significant difficulty in assigning an optical feature to these transitions, double or higher-order excitations might be involved but not considered here.

**Ozone:** the UV-visible absorption spectrum of  $\text{O}_3$  is shown in Figure 6(a), as obtained from the TDDFT calculation, together with the peaks of  $S_{\text{DFT}}(\omega)$

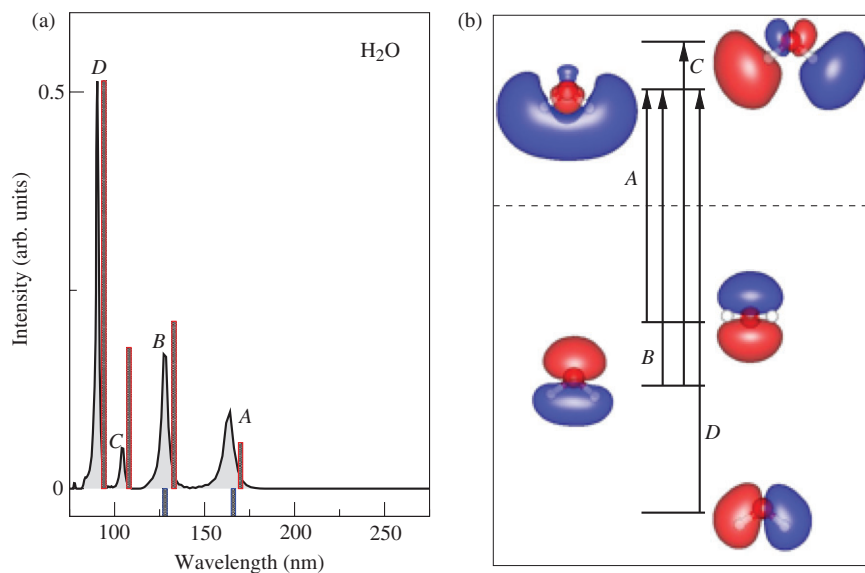


Figure 7. Water molecule: (a) absorption spectrum; (b) energy level diagram (conventions same as in Figure 6).

obtained from DFT, Equation (2), which serve to identify the electronic excitations, as discussed in the previous section. The two sets of peaks follow the same pattern and are reasonably close in energy except for the first peak *A*, with the DFT peaks occurring always at lower energy (higher wavelength), as expected. Four prominent absorption bands are located at 231 nm (5.37 eV), 136 nm (9.14 eV), 113.4 nm (10.93 eV), and 106.6 nm (11.63 eV), all in good agreement with experimental measurements (see Table 2) [1]. The first absorption band, *A*, is a transition from the H-2→LUMO (the HOMO→LUMO excitation is a dark transition). In Figure 6(b), we show the corresponding energy diagram and wavefunctions of different electronic states. The H-2 state consists of  $2p_z$  orbitals from the two end O atoms, while the LUMO results from equal contributions of the three  $2p_z$  orbitals at each O atom. The corresponding TDM shown in Table 2 is oriented along the *y* direction (parallel to the two end O atoms, see Figure 4) for the HOMO-2→LUMO transition. The second absorption band, *B*, is related to electronic excitation from the H-1→L+1 state. The H-1 state is the linear combination of  $2p_x$  and  $2p_y$  orbitals of the two end O atoms in the direction perpendicular to the two O-O bonds. The L+1 is primarily composed of the  $2p_y$  and  $2s$  orbitals from the two end O atoms, and the  $2p_x$  and  $2s$  orbitals from the centre O atom. The TDM for this transition points along the *y* direction, the same as the first peak. A relatively small absorption peak, *C*, appears at 113.4 nm, which is attributed to the H-5→LUMO transition. Both states comprise the  $2p_z$  of three O

atoms: for the H-5, the centre O atom dominates and forms strong  $\pi$  bonds with the other two O atoms, while the LUMO is the linear combination of three  $2p_z$  orbitals, which form the antibonding state. Therefore, the transition has  $\pi \rightarrow \pi^*$  character, associated with electronic redistribution along the *x* direction. The sharp absorption peak, *D*, at 106.6 nm is ascribed to the contribution from the HOMO→L+2 transition. The HOMO is primarily composed of the  $2s$  and  $2p_x$  of the three O atoms, while the L+2 is the combination of the  $2s$ ,  $2p_x$  and  $2p_y$  orbitals, with the  $2p_y$  orbital of the centre O atom being dominant. Accordingly, the orbital arrangement gives a TDM along the *y* direction. It is interesting to note that the TDM in  $O_3$  is always aligned along the *y* direction parallel to the line joining the two end O atoms except for the third band, labelled *C* in Figure 6(a), which is rather weak.

**Water:** the  $H_2O$  molecule exhibits four major absorption bands with wavelength in the range of 80 to 250 nm, shown in Figure 7(a), together with the DFT peaks of  $S_{DFT}(\omega)$ , which in the case of this molecule happen to be in rather good agreement. The first two peaks are at 164.2 nm (7.553 eV) and 127.9 nm (9.740 eV), respectively. In experiment, the primary photoabsorption peaks of gaseous  $H_2O$  are centred at 7.447 and 9.672 eV [2], in excellent agreement with our calculations. The oscillator strength for the first peak, calculated at 0.036, is also very close to the experimental value of 0.03 [56]. The other two peaks in our calculation are located in the higher energy region: at 104.5 nm (11.926 eV) and 90.3 nm (13.715 eV), respectively. They are mixed with the Rydberg series with

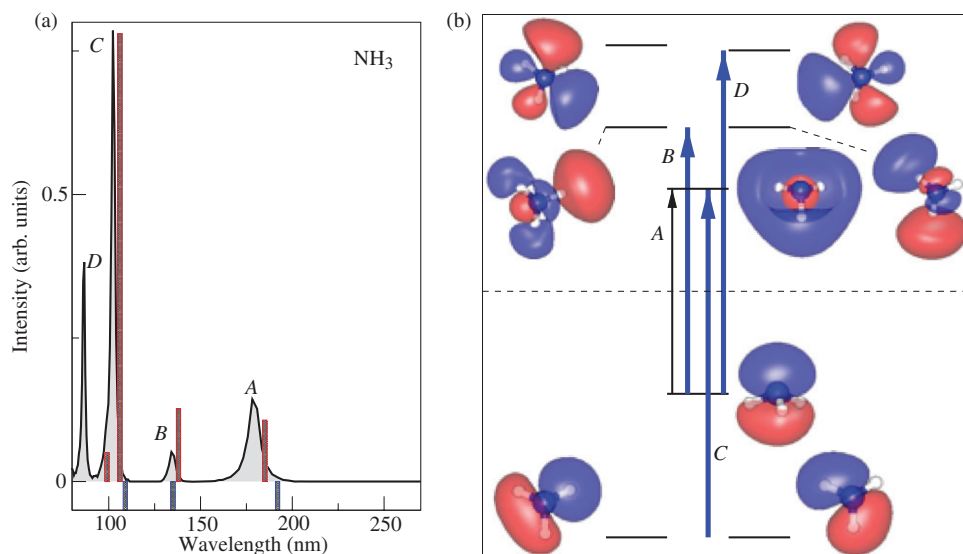


Figure 8. Ammonia molecule: (a) absorption spectrum; (b) energy level diagram (conventions same as in Figure 6).

significant vibronic features in experimental measurements. In order to demonstrate the relationship between optical absorption and the electronic structure, we explore in detail the relevant state transitions in water, as shown in Figure 7(b). The first absorption peak, *A*, is attributed to the HOMO→LUMO transition. The HOMO, often referred to as the  $1B_1$  molecular orbital, is primarily composed of O  $2p_z$  orbitals. The LUMO, the  $4A_1$  orbital, however, is primarily composed of the  $1s$  orbital from the two H atoms and the  $2s$ ,  $2p_x$ , and  $2p_y$  orbitals from the O atom, with the H  $1s$  contribution being dominant. Therefore, the first absorption peak has  $1B_1 \rightarrow 4A_1$  character. The calculated TDM in Table 3 shows that the orientation of the electronic arrangement aligns along the  $z$  direction. The second absorption band, *B*, is ascribed to the H-1→LUMO transition. The electronic orbital assignment of the H-1 state, the  $3A_1$  orbital, is similar to the LUMO, except that the linear combination has equal contributions from all orbitals. Therefore, the second absorption peak corresponds to the  $3A_1 \rightarrow 4A_1$  transition. From the TDM analysis we find that the electrons are polarised along the diagonal direction of the  $x$ - $y$  plane. The third peak, *C*, in Figure 7(a) results from the contribution of electron excitation from the H-1→L+1 state. In the L+1 state, with  $2B_2$  character, the  $1s$  orbital of the two H atoms also dominates the wavefunction, in combination with the contributions from O  $2p_x$  and  $2p_y$  orbitals. In the H-1→L+1 transition, which has  $3A_1 \rightarrow 2B_2$  character, the electron is distributed on the diagonal direction in the  $x$ - $y$  plane with a change of sign in the  $x$  direction. The fourth absorption peak, *D*, is related to the

H-2→LUMO transition. The H-2,  $1B_2$  orbital, is the linear conformation of the H  $1s$ , O  $2p_x$ , and O  $2p_y$  orbitals. The orientation of electronic charge of H<sub>2</sub>O for the  $1B_2 \rightarrow 4A_1$  transition is located in the diagonal of the  $x$ - $(-y)$  plane.

**Ammonia:** by direct electronic excitation, NH<sub>3</sub> absorbs only UV light, in the range of 80–200 nm, as shown in Figure 8(a). The calculated absorption peaks are located at 6.96, 9.24, 12.13 and 14.31 eV, in good agreement with experimental values, reported at 6.46, 9.18, 11.37 eV [7]. The first peak, *A*, with a calculated oscillator strength of 0.053 (experiment [7]: 0.045), comes from the HOMO→LUMO excitation, with the TDM exclusively along the  $z$  direction, that is, the three-fold symmetry axis of the molecule (see Figure 4). There are two degenerate states for each of the H-1, L+1 and L+2 levels. As a result, the other three peaks come from two channels of excitations between these doubly-degenerate states and the single HOMO and LUMO states. It is interesting to compare the wavefunctions of isoelectronic molecules H<sub>2</sub>O and NH<sub>3</sub>: the main features of their wavefunctions are similar, but the degeneracies are different. Consequently, the peak positions (energy separation between states) and the corresponding intensity (state degeneracy) in the UV spectra are also modified. More specifically, the HOMO of NH<sub>3</sub> is dominated by the  $2p_z$  (lone-pair) orbital of N, just as the HOMO of H<sub>2</sub>O was dominated by the  $2p_z$  orbital of O. Similarly, the LUMO of NH<sub>3</sub> has dominant contribution from the three  $1s$  orbitals of H, by analogy to the LUMO character of H<sub>2</sub>O. The other states of NH<sub>3</sub> involve

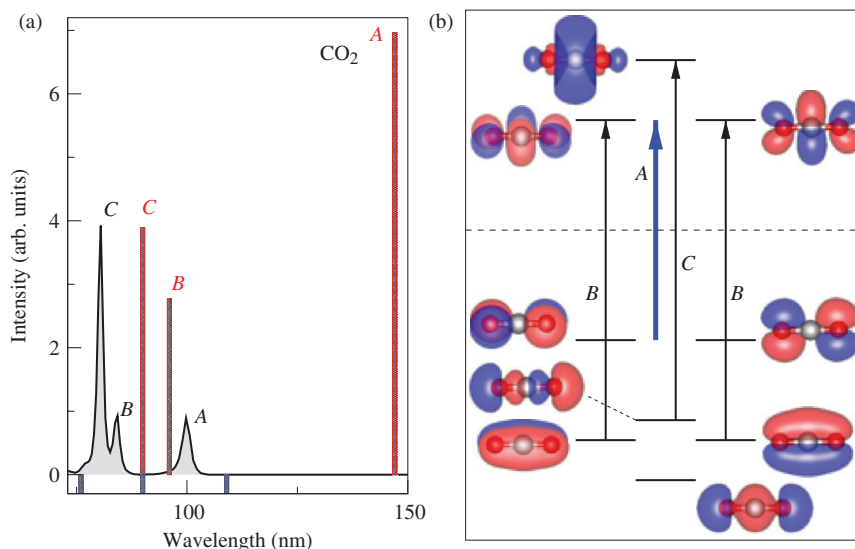


Figure 9. Carbon dioxide molecule: (a) absorption spectrum; (b) energy level diagram (conventions same as in Figure 6).

linear combinations of the  $2p_x$  and  $2p_y$  orbitals of N and the  $1s$  orbitals of H, and as a result the corresponding transitions have TDMs with only  $x$  or  $y$  components (see Table 3).

**Carbon dioxide:** the UV absorption spectrum of CO<sub>2</sub> is shown in Figure 9(a) in the range of 80 to 150 nm, which is in good agreement with experimental data [4]. The first absorption peak, *A*, is centred at 99.8 nm (12.42 eV), which corresponds to the HOMO→LUMO transition. The oscillator strength is 0.293, while corresponding experimental results range from 0.16 to 0.4 [4,60]. Based on the wavefunctions of CO<sub>2</sub>, shown in Figure 9(b), the degenerate HOMO states are primarily composed of the  $2p_x$  and  $2p_y$  orbitals of O atoms, while the LUMO, with anti-bonding character, is a linear combination of  $2p_x$  and  $2p_y$  orbitals from C and two O atoms. The TDM in Table 4 demonstrates that electronic orbitals are distributed in the  $z$  direction with four transition channels. Furthermore, the parallel channels (two states lying in the same plane, see vertical transitions from either the left two or the right two states in Figure 9(b)) dominate the electronic excitation from the HOMO to LUMO. The second absorption band, *B*, at 84.3 nm (14.71 eV) is related to the H-3→LUMO transition. The H-3 consists of the C  $2s$ , O  $2s$ , and O  $2p_z$  orbitals. The relevant wavefunction shows that the molecular orbital has  $\sigma$  character. Therefore, the second peak is related to a  $\sigma \rightarrow \pi^*$  transition. In addition, electrons redistribute along  $x$  or  $y$  axis. The third peak, *C*, at 80.5 nm (15.41 eV) is the H-1→L+1 transition. The H-1 comprises the C  $2p_z$ , O  $2s$ , and O  $2p_z$  orbitals, arranged in a  $\sigma^*$  anti-bonding combination between C–O bonds.

The L+1 is similar to the H-3 with the same orbital arrangement of C  $2s$ , O  $2s$ , and O  $2p_z$  orbitals but the C  $2s$  orbital dominates. Therefore, the molecular orbitals form a donut-like shape around the C atom, as shown in Figure 9(b). From the TDM in Table 4, the electronic redistribution is located along the  $z$  direction.

**Benzene:** C<sub>6</sub>H<sub>6</sub> shows very strong absorption in the low energy region, and several peaks in the high energy region of 80 to 120 nm, as shown in Figure 10(a). The first and strongest absorption band, *A*, located at 178.2 nm (6.96 eV), with a calculated oscillator strength of 0.959 (the experimental value [30] is 0.8–1.2) is attributed to the electronic excitation from HOMO→LUMO. There are two degenerate states in each level, shown in Figure 10(b). The four electronic excitation channels between the HOMO and LUMO all contribute to light absorption and have large TDMs of the same magnitude, which leads to the very large, sharp peak at 6.94 eV observed in experiment [53]. The two degenerate states in the HOMO are primarily composed of C  $2p_z$  orbitals, arranged in a  $\pi$  bonding combination among the C atoms. The HOMO wavefunctions of C<sub>6</sub>H<sub>6</sub> show distinct character: the wavefunction is mostly localised on two pairs of C atoms for the first state, and on opposite triplets of C atoms for the second state. In the LUMO, the two degenerate states are also combinations of C  $2p_z$  orbitals: one state is composed of two  $\pi$  bonding orbitals between two pairs of neighbouring C atoms, and two antibonding orbitals at the two remaining C atoms, while the other state has  $\pi$  anti-bonding character among the first two pairs of neighbouring C

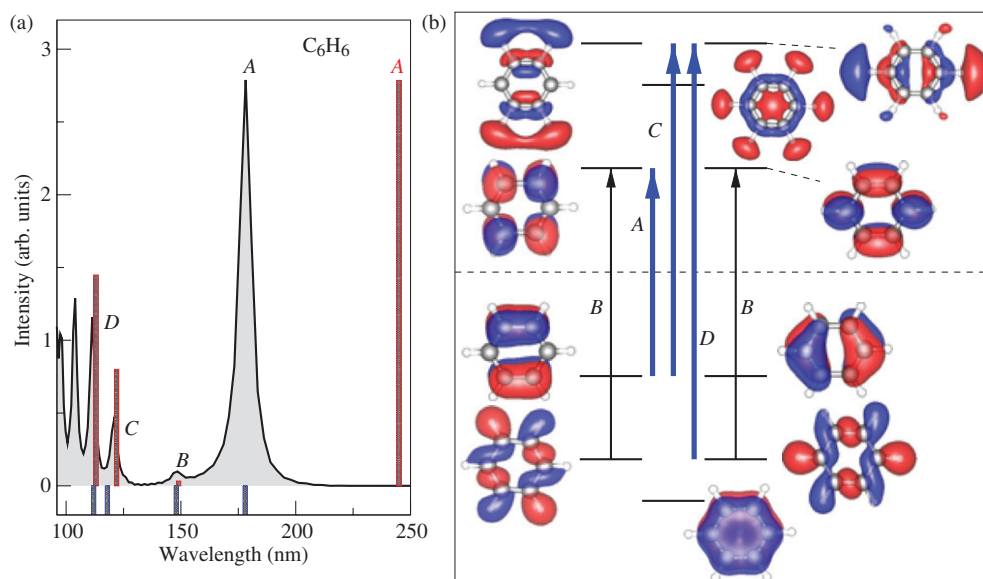


Figure 10. Benzene molecule: (a) absorption spectrum; (b) energy level diagram (conventions same as in Figure 6).

atoms. From the TDM in Table 1, we establish that these electronic transitions of C<sub>6</sub>H<sub>6</sub> involve a TDM primarily along either the  $x$  or the  $y$  direction in the  $x$ - $y$  plane with no  $z$  component. A very small absorption peak,  $B$ , at 148.5 nm (8.35 eV) follows the first band. It is assigned to the H-1 → LUMO transition. The two relevant degenerate states consist of the linear combination of H  $1s$  with C  $2p_x$  and C  $2p_y$  orbitals, respectively. In addition, only two parallel channels (between either the left two or the right two states in Figure 10(b)) in the H-1 → LUMO transition are allowed electronic transitions. From Table 1, they are  $n \rightarrow \pi^*$  transitions with a TDM along the  $z$  axis with a different sign. In Figure 10(a), the third band,  $C$ , at 121.1 nm (10.24 eV), is attributed to the HOMO → L+2 transition. The process is similar to the first absorption band, which involves four electronic excitation channels between two degenerate states. However, the atomic orbital arrangements for the L+2 states are different, as shown in Figure 10(b): one comprises the linear combination of C  $2s$ , C  $2p_x$  with H  $1s$  orbitals, while the other has the same linear combination except for containing the C  $2p_y$  instead of the C  $2p_x$  orbitals. The H  $1s$  orbital dominates the higher unoccupied states. In the HOMO → L+2 transition, the electronic redistribution is along the  $z$  direction ( $\pi \rightarrow n^*$  transitions). The fourth absorption peak,  $D$ , is at 113.4 nm (11.13 eV), originating from H-1 → L+2 transitions, with four electronic excitation channels. It is similar to the first adsorption peak: electron redistribution is along the  $x$  or  $y$  axis with the same signs for the two cross-channels and opposite signs for the parallel channels. Our results of the optical absorption spectra

are in good agreement with the experimental values [53]. Beyond these four peaks, other adsorption bands at 11.93, 12.72, 13.02, 13.81 eV, correspond to the experimental peaks at 12.16, 12.50, 13.00, 14.60 eV, respectively. Compared to quantum chemistry calculations, the quality of the spectra calculated by the present approach clearly surpasses the accuracy of Hartree-Fock approximation, and the use of Gaussian basis 6-311G\*\*, reaching an accuracy comparable to spectra obtained with CASPT2 or TDDFT with hybrid functionals (B3LYP and PBE0) and highly converged Gaussian basis-sets for benzene [25,29,30]. This good agreement might be accidental, however, since generally a TDDFT approach is not superior to quantum chemistry methods at the CASPT2 level.

#### 4. Conclusion

We have obtained the optical absorption spectra of a hydrogen-terminated Si nanocluster of diameter 2 nm as well as fifteen representative small molecules, using a TDDFT approach with a self-consistency condition imposed in the time evolution of electronic states. The results for the Si nanoclusters with and without P dopants clearly demonstrate the efficiency of the method for systems containing several hundred atoms, allowing for accurate predictions of the electronic and optical properties of such systems. The results for the molecular optical absorption spectra are in good agreement with experimental values, in what concerns both the position and magnitude of prominent (bright) peaks, indicating a satisfactory performance of the method, and provide detailed

information on the different contributions of the relevant electronic state transitions. These results are valuable for molecular recognition, either in an ensemble of molecules in thermal equilibrium, or in cases where the molecules have the same excitation energy but different directional adsorption, assuming that they can be aligned in the electric field. The transition dipole moments of these molecules can also be useful in identifying the molecular orientations in cases where the molecules are aligned in an electrostatic field or on a surface due to the presence of a surface potential.

### Acknowledgements

We thank Dr A. Gali for providing us the coordinates of the  $\text{Si}_{220}\text{H}_{144}$  cluster. S.M. acknowledges support from the Hundred-Talent program of CAS.

### Note

All figures can be viewed in colour online.

### References

- [1] N.J. Mason, J.M. Gingell, J.A. Davies, H. Zhao, I.C. Walker and M.R.F. Siggel, *J. Phys. B: Atom. Mol. Opt. Phys.* **29**, 3075 (1996).
- [2] R. Mota, R. Parafita, A. Giuliani, M.-J. Hubin-Franskin, J.M.C. Lourenco, G. Garcia, S.V. Hoffmann, N.J. Mason, P.A. Ribeiro, M. Raposo and P. Lima-Vieira, *Chem. Phys. Lett.* **416**, 152 (2005).
- [3] W.F. Chan, G. Cooper and C.E. Brion, *Chem. Phys.* **180**, 77 (1994).
- [4] W.F. Chan, G. Cooper and C.E. Brion, *Chem. Phys.* **178**, 401 (1993).
- [5] G. Cooper, J.E. Anderson and C.E. Brion, *Chem. Phys.* **209**, 61 (1996).
- [6] F.W. Taylor, *Rep. Prog. Phys.* **65**, 1 (2002).
- [7] M. Suto and L.C. Lee, *J. Chem. Phys.* **78**, 4515 (1983).
- [8] E.E. Koch and A. Otto, *Chem. Phys. Lett.* **12**, 476 (1972).
- [9] J.A. Pople, R. Seeger and R. Krishnan, *Int. J. Quantum Chem. Symp.* **11**, 149 (1977).
- [10] H.G. Kummel, in *Proceedings of the 11th International Conference: Recent Progress in Many-body Theories*, edited by R.F. Bishop, T. Brandes, K.A. Gernoth, N.R. Walet, and Y. Xian (World Scientific Publishing, Singapore, 2002), pp. 334–348.
- [11] K. Andersson, P.A. Malmqvist and B.O. Roos, *J. Chem. Phys.* **96**, 1218 (1992).
- [12] N.N. Matsuzawa, A. Ishitani, D.A. Dixon and T. Uda, *J. Phys. Chem.* **105**, 4953 (2001).
- [13] C. Adamo, G.E. Scuseria and V. Barone, *J. Chem. Phys.* **111**, 2889 (1999).
- [14] P. Hohenberg and W. Kohn, *Phys. Rev.* **136**, B864 (1964).
- [15] W. Kohn and L.J. Sham, *Phys. Rev.* **140**, A1133 (1965).
- [16] E. Runge and E.K.U. Gross, *Phys. Rev. Lett.* **52**, 997 (1984).
- [17] M.E. Casida, C. Jamorski, K.C. Casida and D.R. Salahub, *J. Chem. Phys.* **108**, 4439 (1998).
- [18] R.J. Cave, K. Burke and E.W. Castner Jr, *J. Phys. Chem. A* **106**, 9294 (2002).
- [19] K. Burke, J. Werschnik and E.K.U. Gross, *J. Chem. Phys.* **123**, 062206 (2005).
- [20] B.G. Levine, C. Ko, J. Quenneville and T.J. Martinez, *Mol. Phys.* **104**, 1039 (2006).
- [21] M.E. Casida, in *Recent Developments and Applications in Density Functional Theory*, edited by J.M. Seminario (Elsevier, Amsterdam, 1996).
- [22] N. Santhanamoorthi, K. Senthilkumar and P. Kolandaivel, *Mol. Phys.* **107**, 1629 (2009).
- [23] E. Tapavicza, I. Tavernelli and U. Rothlisberger, *Phys. Rev. Lett.* **98**, 023001 (2007).
- [24] R. Bauernschmitt and R. Ahlrichs, *Chem. Phys. Lett.* **256**, 454 (1996).
- [25] R.E. Stratmann, G.E. Scuseria and M.J. Frisch, *J. Chem. Phys.* **109**, 8218 (1998).
- [26] F. Furche and R. Ahlrichs, *J. Chem. Phys.* **117**, 7433 (2002).
- [27] M. Parac and S. Grimme, *Chem. Phys.* **292**, 11 (2003).
- [28] R. Bauernschmitt, M. Haser, O. Treutler and R. Ahlrichs, *Chem. Phys. Lett.* **264**, 573 (1996).
- [29] S.J.A. van Gisbergen, A. Rosa, G. Ricciardi and E.J. Baerends, *J. Chem. Phys.* **111**, 2499 (1999).
- [30] M. Miura, Y. Aoki and B. Champagne, *J. Chem. Phys.* **127**, 084103 (2007).
- [31] M. Parac and S. Grimme, *J. Phys. Chem. A* **106**, 6844 (2002).
- [32] M.A.L. Marques, C.A. Ullrich, F. Nogueira, A. Rubio, K. Burke and E.K.U. Gross, *Time-Dependent Density Functional Theory* (Springer, Berlin, 2006).
- [33] K. Yabana and G.F. Bertsch, *Phys. Rev. B* **54**, 4484 (1996).
- [34] O. Sugino and Y. Miyamoto, *Phys. Rev. B* **59**, 2579 (1999).
- [35] A. Castro, M.A.L. Marques and A. Rubio, *J. Chem. Phys.* **121**, 3425 (2004).
- [36] I. Tavernelli, U.F. Rohrig and U. Rothlisberger, *Mol. Phys.* **103**, 963 (2005).
- [37] D. Rocca, R. Gebauer, Y. Saad and S. Baroni, *J. Chem. Phys.* **128**, 154105 (2008).
- [38] M.A.L. Marques, A. Castro, and A. Rubio, The octopus manual. <http://www.tddft.org/programs/octopus/>
- [39] C. Hu, O. Sugino and Y. Miyamoto, *Phys. Rev. A* **74**, 032508 (2006).
- [40] J.M. Soler, E. Artacho, J.D. Gale, A. García, J. Junquera, P. Ordejón and D. Sánchez-Portal, *J. Phys.: Condens. Matter* **14**, 2745 (2002).
- [41] N. Troullier and J.L. Martins, *Phys. Rev. B* **43**, 1993 (1991).

- [42] D.M. Ceperley and B.J. Alder, *Phys. Rev. Lett.* **45**, 566 (1980).
- [43] J.P. Perdew and A. Zunger, *Phys. Rev. B* **23**, 5048 (1981).
- [44] E. Artacho, D. Sánchez-Portal, P. Ordejón, A. García and J.M. Soler, *Phys. Stat. Sol. B* **215**, 809 (1999).
- [45] A. Tsolakidis, D. Sánchez-Portal and R.M. Martin, *Phys. Rev. B* **66**, 235416 (2002).
- [46] A. Tsolakidis and E. Kaxiras, *J. Phys. Chem. A* **109**, 2373 (2005).
- [47] S. Meng and E. Kaxiras, *J. Chem. Phys.* **129**, 054110 (2008).
- [48] A.T. Al-Kazwini, P. O'Neill, R.B. Cundall, G.E. Adams, A. Junino and J. Maignan, *Tetrahedron Lett.* **33**, 3045 (1992).
- [49] V.P. Grishchuk, S.A. Davidenko, I.D. Zholner, A.B. Verbitskii, M.V. Kurik and Y.P. Piryatinskii, *Tech. Phys. Lett.* **28**, 36 (2002).
- [50] T.L. Chan, M.L. Tiago, E. Kaxiras and J.R. Chelikowsky, *Nano Lett.* **8**, 596 (2008).
- [51] A. Tsolakidis and R.M. Martin, *Phys. Rev. B* **71**, 125319 (2005).
- [52] I. Vasiliev, S. Ogut and J.R. Chelikowsky, *Phys. Rev. Lett.* **86**, 1813 (2001).
- [53] E.E. Koch and M. Skibowski, *Chem. Phys. Lett.* **9**, 429 (1971).
- [54] G. Cooper, T. Ibuki, Y. Iida and C.E. Brion, *Chem. Phys.* **125**, 307 (1988).
- [55] G. Cooper, T.N. Olney and C.E. Brion, *Chem. Phys.* **194**, 175 (1985).
- [56] P.G. Wilkison and H.L. Johnston, *J. Chem. Phys.* **18**, 190 (1950).
- [57] R. van Harrevelt, *J. Chem. Phys.* **126**, 204313 (2007).
- [58] K. Yoshino, J.R. Esmond and W.H. Parkinson, *Chem. Phys.* **221**, 169 (1997).
- [59] T. Nakayama, M.Y. Kitamura and K. Watanabe, *J. Chem. Phys.* **30**, 1180 (1959).
- [60] J.W. Rabalais, J.M. McDonald, V. Scherr and S.P. McGlynn, *Chem. Rev.* **71**, 73 (1971).